CrystEngComm

RSC Publishing

COMMUNICATION

View Article Online
View Journal | View Issue

Accessing functionalized porous aromatic frameworks (PAFs) through a *de novo* approach†

Cite this: *CrystEngComm*, 2013, **15**, 1515

Received 1st October 2012,
Accepted 18th October 2012

DOI: 10.1039/c2ce26595h

www.rsc.org/crystengcomm

Sergio J. Garibay,[a] Mitchell H. Weston,[a] Joseph E. Mondloch,[a] Yamil J. Colón,[b] Omar K. Farha,*[a] Joseph T. Hupp*[a] and SonBinh T. Nguyen*[a]

Methyl-, hydroxymethyl-, and phthalimidomethyl-functionalized versions of the porous organic polymer PAF-1 have been obtained through *de novo* synthesis. The CO_2 adsorption capacity of PAF-1–CH_2NH_2, obtained through the post-synthesis deprotection of PAF-1–CH_2–phthalimide, has been shown to exceed that of PAF-1.

Introduction

There has been significant recent interest in microporous organic polymeric (POP) materials due to advances in their synthesis[1] and recognition of their potential applications in catalysis,[2] gas storage and release,[3] and chemical separations.[4] New synthesis strategies involving self-condensation or cross-coupling reactions have led to a variety of POPs,[4–6] including crystalline or semi-crystalline covalent organic frameworks,[7,8] and triazine-based organic frameworks,[9] as well as amorphous polymers of intrinsic microporosity,[10] hyper-crosslinked polymers,[11] and conjugated microporous polymers.[12] One of the most exciting recent developments has been the synthesis of POPs possessing extraordinarily high surface areas *via* the Yamamoto–Ullmann cross-coupling of tetrakis(4-bromophenyl)methane monomers (Scheme 1).[13–18] Indeed, the most porous versions, **PAF-1** and **PAF-3** (PAF = porous aromatic framework), display Brunauer–Emmett–Teller (BET) surface areas of up to 5600[14] and 6461 $m^2\ g^{-1}$,[19] with the latter, until recently,[20] being the material with the highest known surface area. Because PAF materials feature tetrahedral atomic or small-molecular nodes and simple (unsubstituted) biphenyl units as struts, they have been approximately formulated as diamondoid networks (albeit, without compelling evidence for long-range order). Their exceptional porosities are attributable to an apparent lack of catenation, a rarity for POPs as well as MOFs (metal–organic frameworks) based on diamondoid networks. Although **PAF-1** and its derivatives have shown impressive adsorption capacities for H_2 and CH_4,[16,19] the absence of functional groups, however, renders them relatively nonspecific as sorbents for small, functionalized molecules.

Recently, Zhou and co-workers have reported the post-synthesis modification (PSM) of **PAF-1** to yield sulfonated[21] and chloromethyl[22] derivatives, the latter can be further modified to tether amine groups within the pores of the diamondoid PAF network. While these functional groups led to enhanced gravimetric CO_2 uptake, the extent that a PAF particle can be post-synthetically modified greatly depends on the ability of the reagents to penetrate its whole morphological structure. As a result, inhomogeneity may very well exist in a PAF particle that has been subjected to PSM where the outer "shell" would be more highly functionalized than the inner "core". Presumably, this situation would not exist if functionalized **PAF-1** derivatives can be directly synthesized from the corresponding functionalized monomers in a *de novo* fashion.

Herein, we describe the *de novo* syntheses of methyl-, hydroxymethyl-, and phthalimidomethyl-substituted **PAF-1** derivatives (Scheme 2). From the latter, amine- and imine-containing

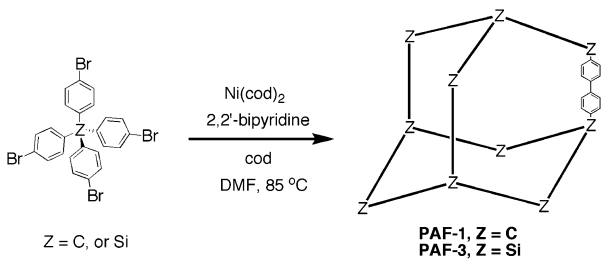

Scheme 1 The synthesis of **PAF-1** and **PAF-3** (Z = C or Si, respectively) from the corresponding functionalized tetrakis(4-bromophenyl) methane tetrahedral building units. The PAF framework is schematically represented as an adamantane cage.

[a]*Department of Chemistry and International Institute for Nanotechnology, Northwestern University, 2145 Sheridan Road, Evanston, IL, 60208, USA. E-mail: o-farha@northwestern.edu; j-hupp@northwestern.edu; stn@northwestern.edu; Fax: +1 847-467-1425; Fax: +1 847-491-7713; Tel: +1 847-467-4934 Tel: +1 847-491-3504 Tel: +1 847-467-3347*

[b]*Department of Chemical and Biological Engineering, Northwestern University, 2145 Sheridan Road, Evanston, IL, 60208-3120, USA*

† Electronic supplementary information (ESI) available: Synthetic details and characterization data for all compounds and materials. See DOI: 10.1039/c2ce26595h

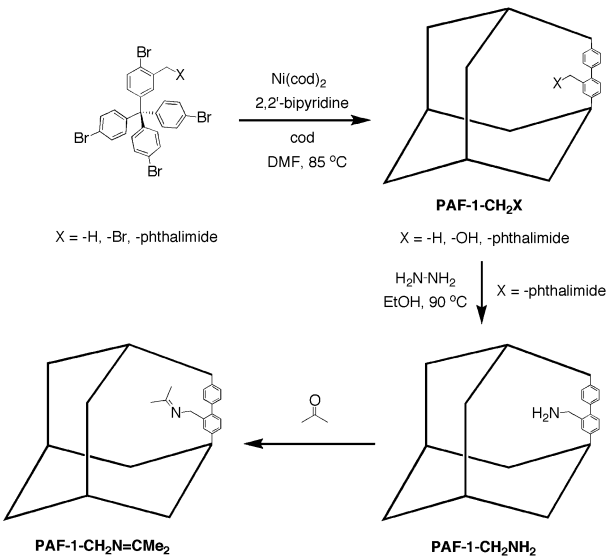

Scheme 2 Top: the *de novo* synthesis of **PAF-1–CH_3**, **PAF-1–CH_2OH**, and **PAF-1–CH_2–phthalimide** (X = H, OH, or phthalimide, respectively) from the corresponding functionalized tetrakis(4-bromophenyl) methane tetrahedral building units. Bottom: the post-synthesis deprotection of **PAF-1–CH_2–phthalimide** with hydrazine to give **PAF-1–CH_2NH_2**, which can then react with acetone to afford **PAF-1–CH_2N=CMe_2**. The **PAF-1** framework is schematically represented as an adamantane cage.

PAF-1-based materials can be easily obtained through post-synthesis deprotection (PSD),[23] thus greatly expanding the range of available functionalized **PAF-1** derivatives. The versatile combination of *de novo* synthesis and PSD chemistry allows us to readily tune the pore environment in **PAF-1** for CO_2 absorption: the amine-containing **PAF-1** derivative exhibits high affinities for CO_2, while the materials with less-basic pore environments do not bind CO_2 as strongly.

Results and discussion

The syntheses of –CH_3, –CH_2OH, and –CH_2–phthalimide **PAF-1** derivatives were carried out by coupling together the appropriately modified tetrakis(4-bromophenyl)methane building units in the presence of a Ni(0) reagent following a modified procedure reported by Zhu and co-workers (see ESI† and Scheme 1).[14] As in the synthesis of **PAF-1**, these reactions all produced off-white powdered materials that were insoluble in common organic solvents. Their solid-state ^{13}C CP-MAS NMR spectra (Section V in the ESI†) all contain signals that are consistent with the aromatic and quaternary carbons of **PAF-1**. Although the benzylic carbon resonance for **PAF-1–CH_2OH** overlaps with the quarternary node carbon (Fig. S10 in the ESI†), it is quite prominent for **PAF-1–CH_3** (δ = 17 ppm, Fig. S9 in the ESI†) and **PAF-1–CH_2–phthalimide** (δ = 39 ppm, Fig. S11 in the ESI†). In addition, the spectrum of **PAF-1–CH_2–phthalimide** contains a pronounced carbonyl resonance (δ = 166 ppm) that can be attributed to the C=O moiety of the phthalimide functional group.

Although we initially intended to produce **PAF-1–CH_2Br** from polymerizing the corresponding bromomethyl-functionalized tetrahedral building unit, the benzylic bromide moiety did not survive the reaction and the work up. Instead, **PAF-1–CH_2OH** was obtained. This assignment was supported by the lack of the characteristic benzyl bromide carbon resonance (δ ~33 ppm) in the solid-state ^{13}C CP-MAS NMR spectrum of this material (Fig. S10 in the ESI†) as well as its elemental analysis data, which shows a significant oxygen content and only trace amounts of bromine (Table S1 in the ESI†). Presumably, the benzyl bromide moieties were hydrolyzed during the highly acidic work-up (with concentrated HCl) of the reaction. Consistent with this assignment, the FTIR spectrum of **PAF-1–CH_2OH** (Fig. S15 in the ESI†) contains stretches at 3417 cm^{-1} that can be attributed to the hydroxy methyl functionality.

The **PAF-1** derivatives are generally much less stable than the parent **PAF-1** material: their thermogravimetric analysis (TGA) profiles under nitrogen (Fig. S16 in the ESI†) shows mass losses due to decomposition at around 300–400 °C, much lower than the expected 520 °C of **PAF-1**.[14] As expected, **PAF-1–CH_3** and **PAF-1–CH_2OH** are more stable than **PAF-1–CH_2–phthalimide**.

The presence of functional groups in the PAF diamondoid cavity results in decreases in BET surface areas and pore diameters (Fig. S17 in the ESI†) of the –CH_3, –CH_2OH, and –CH_2–phthalimide **PAF-1** derivatives, as shown by their N_2 adsorption profiles at 77 K (Fig. 1 and Table 1). As expected, the –CH_3 and –CH_2OH derivatives have total NLDFT-derived pore and micropore volumes that are comparable to those for the parent **PAF-1** while the values for the –CH_2–phthalimide derivative are much smaller. Notably, the NLDFT-derived bulk densities of the –CH_3 and –CH_2OH derivatives, as measured by helium pycnometry, are quite similar to that of the parent **PAF-1** (see Table S2 and the associated discussion in the ESI†), suggesting that their networks are probably non-catenated, as in **PAF-1**.

The generation and utilization of benzylamine functionalities within the **PAF-1** framework was accomplished through PSM

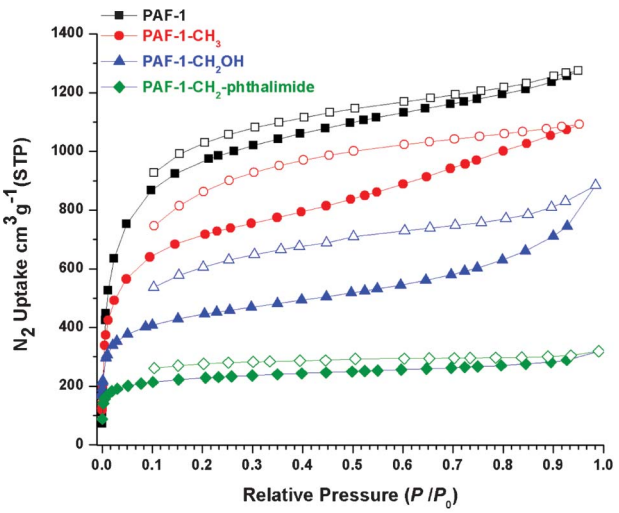

Fig. 1 N_2 isotherms of **PAF-1**, **PAF-1–CH_3**, **PAF-1–CH_2OH**, and **PAF-1–CH_2–phthalimide** measured at 77 K. Closed symbols = adsorption; open symbols = desorption.

Table 1 Pore and surface properties of **PAF-1** derivatives

PAF derivatives	BET surface area[a] ($m^2\ g^{-1}$)	Total pore volume[b] ($cm^3\ g^{-1}$)	Dominant NLDFT-calcd. pore diameter[c] (Å)	CO_2 uptake[d] ($cm^3\ g^{-1}$)
PAF-1	4100	2.23 (0.86)[e]	13.6	55.1
PAF-1–CH_3	3007	2.01 (0.62)[e]	12.5	55.0
PAF-1–CH_2OH	1727	1.77 (0.33)[e]	12.2	66.8
PAF-1–CH_2–phthalimide	974	0.58 (0.26)[e]	11.8	50.1
PAF-1–CH_2NH_2	1363	0.74 (0.37)[e]	11.7	98.0
PAF-1–CH_2N=CMe_2	1302	0.73 (0.37)[e]	11.7	70.1

[a] Calculated in the range of $0.01 < (p/p_0) < 0.1$. The results are averages from at least two independent experiments. [b] Total pore volume at $p/p_0 = 0.98$. [c] Maxima of the pore size distribution calculated using the NLDFT method and slit-pore model. [d] Measured at 273 K. [e] This is the total micropore volume ($cm^3\ g^{-1}$) determined by the NLDFT method.

(Scheme 2). After refluxing **PAF-1–CH_2–phthalimide** with an ethanolic solution of hydrazine hydrate for 48 h, the recovered material was washed with DMSO and DMF and Soxhlet-extracted with ethanol to remove the phthalhydrazide byproduct. The solid-state ^{13}C CP-MAS NMR spectrum of **PAF-1–CH_2–phthalimide** (Fig. S11 in the ESI†) significantly changes after hydrazine treatment. Notably, the pronounced carbonyl resonance (δ = 166 ppm) associated with the C=O moiety of the phthalimide functional group is eliminated while a new resonance (δ = 46 ppm) corresponding to the benzylic CH_2NH_2 appears, indicative of successful deprotection. FTIR spectroscopy additionally provides evidence of deprotection and conversion into **PAF-1–CH_2NH_2**: after hydrazine treatment, the carbonyl stretches at 1774 and 1721 cm^{-1}, attributed to the phthalimide functionality, become diminished and characteristic amine (N–H) stretches at 3383 and 3305 cm^{-1} emerge (Fig. S15 in the ESI†). Removal of the bulky phthalimide groups from the **PAF-1–CH_2–phthalimide** network was found to greatly enhance N_2 uptake, resulting in greater surface areas and the total pore volume (Fig. 2 and Table 1).

The benzylic amine group in **PAF-1–CH_2NH_2** can be readily converted into an imine *via* room-temperature reaction with acetone. The solid-state ^{13}C CP-MAS NMR spectrum of the imine-functionalized derivative **PAF-1–CH_2N=CMe_2** (Fig. S13 in the ESI†) exhibited a new N=C(CH_3)$_2$ resonance (δ = 30 ppm) and an imine N=CMe_2 resonance (δ = 166 ppm). Although the benzylic resonance of the CH_2N=CMe_2 moiety overlaps with that of the quaternary node carbon (δ = 64 ppm), the benzylic resonance of the initial CH_2NH_2 (δ = 46 ppm) moiety completely disappears, suggesting complete conversion. The FTIR spectrum of **PAF-1–CH_2N=CMe_2** (Fig. S14 in the ESI†) contains a stretch at 1669 cm^{-1} that can be attributed to the imine functionality. As the imine substituents in **PAF-1–CH_2N=CMe_2** are relatively small, its N_2 adsorption properties are similar to that of the parent **PAF-1–CH_2NH_2**, with comparable surface areas and pore volume (Table 1).

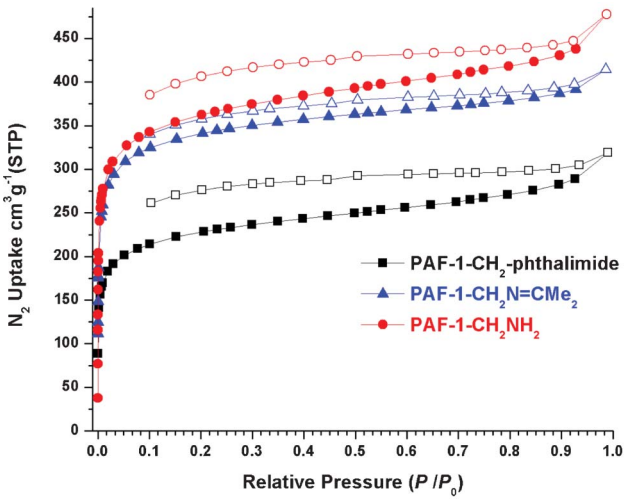

Fig. 2 N_2 isotherms for **PAF-1–CH_2–phthalimide**, **PAF-1–CH_2N=CMe_2**, and **PAF-1–CH_2NH_2** measured at 77 K. Closed symbols = adsorption; open symbols = desorption.

The incorporation of Lewis-basic functionalities (especially alkyl amines) into porous materials has increasingly been explored for applications in CO_2 separation.[24] Recent reports utilizing amine-tethered porous materials have demonstrated enhanced and selective CO_2 adsorption as a consequence of the high affinities of amines for CO_2.[22] Not surprisingly, while the CO_2 adsorption capacity of **PAF-1–CH_3** is similar to that of **PAF-1**, our Lewis-basic hydroxymethyl and imine derivatives have 21 and 27% more enhanced adsorption capacities, respectively. The introduction of aminomethyl groups into **PAF-1** resulted in outstanding CO_2 adsorption: the loading capacity of **PAF-1–CH_2NH_2** was almost double that of **PAF-1** (98 *vs.* 55 $cm^3\ g^{-1}$) at 1 bar and 273 K (Table 1 and Fig. 3). As expected, the isosteric heat of adsorption (Q_{st}) increases from the original 15.6 kJ mol^{-1} value for **PAF-1** to 18.2 kJ mol^{-1} for **PAF-1–CH_2N=CMe_2** and 19.3 kJ mol^{-1} for **PAF-1–CH_2OH**, and to 57.6 kJ mol^{-1} for **PAF-1–CH_2NH_2** (Fig. S21 in the ESI†). This last calculated Q_{st} value is consistent with that obtained ($\sim$55 kJ mol^{-1}) for the polyamine-tethered PAF derivative **PPN-6-CH_2DETA**,[22] which possesses a slightly higher level ($\sim$0.3 N per phenyl ring) of amine functionalization than ours ($\sim$0.25 N per phenyl ring).

Interestingly, the ability of our **PAF-1–CH_2OH** derivative to uptake small molecules such as ethanol and toluene (Fig. S18 and S19 in the ESI†) appears to be mostly a function of sterics. While both **PAF-1** and **PAF-1–CH_2OH** can uptake ethanol (32.6 and 26.6 mmol g^{-1}, respectively) and toluene (18.2 and 14.3 mmol g^{-1}, respectively), **PAF-1–CH_2OH** has a slightly lower uptake, presumably due to its relatively lower pore volume. The inherent hydrophobicity of the aromatic PAF framework minimizes the

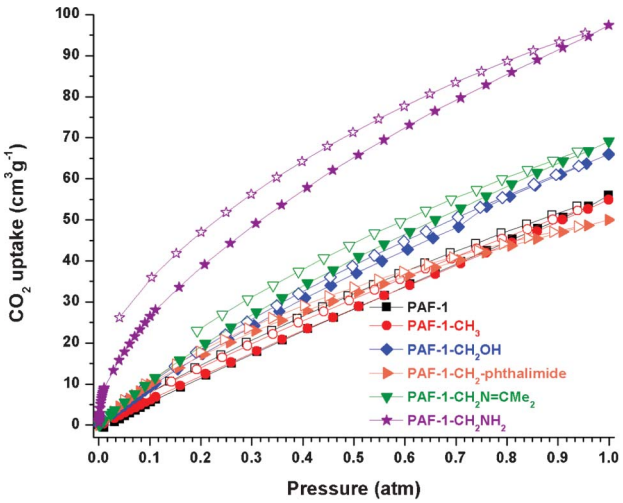

Fig. 3 CO_2 isotherms for **PAF-1** derivatives measured at 273 K. Closed symbols = adsorption; open symbols = desorption.

capacity of both materials to uptake water. Nevertheless, at this low level of uptake **PAF-1–CH_2OH** adsorbs a slightly larger amount of water than **PAF-1** (1 *vs.* 0.72 mmol g^{-1}, Fig. S20 in the ESI†), presumably due to its ability to better hydrogen-bond to water.

Conclusions

In summary, we have synthesized and characterized –CH_3, –CH_2OH, and –CH_2–phthalimide derivatives of **PAF-1** *via* the Yamamoto–Ullmann cross-coupling of singly functionalized derivatives of the tetrakis(4-bromophenyl) methane building unit. **PAF-1–CH_2–phthalimide** can be successfully converted into **PAF-1–CH_2NH_2**, and then **PAF-1–CH_2N=CMe_2** through PSM. In spite of the relatively low level of functionalization (25% of the aromatic groups), the amine functionalities in **PAF-1–CH_2NH_2** were found to significantly enhance its CO_2 adsorption capacity relative to the parent **PAF-1**. Together, these results demonstrate that functionalized derivatives of the **PAF-1** framework with tunable physical properties can be readily synthesized in a *de novo* fashion. Given the extensive use of alcohol- and amine-based PSM in the related area of MOF chemistry, **PAF-1–CH_2OH** and **PAF-1–CH_2NH_2** can readily serve as platforms for incorporating site-specific functionalities for new applications in separations and catalysis.

Acknowledgements

This work was supported by the Dow Chemical Company. We additionally thank the Department of Energy (DOE) Office of Energy Efficiency and Renewable Energy (EERE) for supporting the gas sorption measurements and analyses (grant no. DE-FG36-08GO18137/A001). J. E. M. is supported in part by the DOE-EERE Postdoctoral Research Awards under the EERE Fuel Cell Technologies Program administered by ORISE for the DOE. M. H. W. is supported in part by DTRA (agreement HDTRA1-10-1-0023). Y. J. C. is an NSF Graduate Research Fellow (grant no. DGE-0824162). We thank Prof. Randall Q. Snurr, Dr. Kurt Hirsekorn, and Dr. Rui Cruz for helpful discussions; Dr. Yuyang Wu for assistance with solid-state NMR measurements; Ms. Prativa Pandey for assistance with pore-size distribution analysis; and Dr. Kenji Sumida and Mr. Zachary Brown for assistance with the CO_2 Q_{st} calculations.

Instruments in the Northwestern University Integrated Molecular Structure Education and Research Center (IMSERC) were purchased with grants from NSF-NSEC, NSF-MRSEC, Keck Foundation, the state of Illinois, and Northwestern University.

References

1 R. Dawson, A. I. Cooper and D. J. Adams, *Prog. Polym. Sci.*, 2012, **37**, 530–563.
2 Y. Zhang and S. N. Riduan, *Chem. Soc. Rev.*, 2012, **41**, 2083–2094.
3 W. Lu, D. Yuan, D. Zhao, C. I. Schilling, O. Plietzsch, T. Muller, S. Bräse, J. Guenther, J. Blümel, R. Krishna, Z. Li and H. C. Zhou, *Chem. Mater.*, 2010, **22**, 5964–5972.
4 O. K. Farha, Y.-S. Bae, B. G. Hauser, A. M. Spokoyny, R. Q. Snurr, C. A. Mirkin and J. T. Hupp, *Chem. Commun.*, 2010, **46**, 1056–1058.
5 O. K. Farha, A. M. Spokoyny, B. G. Hauser, Y.-S. Bae, S. E. Brown, R. Q. Snurr, C. A. Mirkin and J. T. Hupp, *Chem. Mater.*, 2009, **21**, 3033–3035.
6 A. M. Shultz, O. K. Farha, J. T. Hupp and S. T. Nguyen, *Chem. Sci.*, 2011, **2**, 686–689.
7 H. M. El-Kaderi, J. R. Hunt, J. L. Mendoza-Cortés, A. P. Côté, R. E. Taylor, M. O'Keeffe and O. M. Yaghi, *Science*, 2007, **316**, 268–272.
8 X. Feng, X. Ding and D. Jiang, *Chem. Soc. Rev.*, 2012, **41**, 6010–6022.
9 P. Kuhn, M. Antonietti and A. Thomas, *Angew. Chem., Int. Ed.*, 2008, **47**, 3450–3453.
10 N. B. McKeown and P. M. Budd, *Chem. Soc. Rev.*, 2006, **35**, 675–683.
11 C. D. Wood, B. Tan, A. Trewin, H. Niu, D. Bradshaw, M. J. Rosseinsky, Y. Z. Khimyak, N. L. Campbell, R. Kirk, E. Stöckel and A. I. Cooper, *Chem. Mater.*, 2007, **19**, 2034–2048.
12 J. X. Jiang, F. Su, A. Trewin, C. D. Wood, N. L. Campbell, H. Niu, C. Dickinson, A. Y. Ganin, M. J. Rosseinsky, Y. Z. Khimyak and A. I. Cooper, *Angew. Chem., Int. Ed.*, 2007, **46**, 8574–8578.
13 T. Ben and S. Qiu, *CrystEngComm.*, 2012, DOI: 10.1039/C2CE25409C.
14 T. Ben, H. Ren, S. Ma, D. Cao, J. Lan, X. Jing, W. Wang, J. Xu, F. Deng, J. M. Simmons, S. Qiu and G. Zhu, *Angew. Chem., Int. Ed.*, 2009, **48**, 9457–9460.
15 Y. Peng, T. Ben, J. Xu, M. Xue, X. Jing, F. Deng, S. Qiu and G. Zhu, *Dalton Trans.*, 2011, **40**, 2720–2724.
16 T. Ben, C. Pei, D. Zhang, J. Xu, F. Deng, X. Jing and S. Qiu, *Energy Environ. Sci.*, 2011, **4**, 3991–3999.
17 H. Ren, T. Ben, F. Sun, M. Guo, X. Jing, H. Ma, K. Cai, S. Qiu and G. Zhu, *J. Mater. Chem.*, 2011, **21**, 10348–10353.
18 Y. Yuan, F. Sun, H. Ren, X. Jing, W. Wang, H. Ma, H. Zhao and G. Zhu, *J. Mater. Chem.*, 2011, **21**, 13498–13502.
19 D. Yuan, W. Lu, D. Zhao and H. C. Zhou, *Adv. Mater.*, 2011, **23**, 3723–3725.
20 O. K. Farha, I. Eryazici, N. C. Jeong, B. G. Hauser, C. E. Wilmer, A. A. Sarjeant, R. Q. Snurr, S. T. Nguyen, A. Ö. Yazaydin and J. T. Hupp, *J. Am. Chem. Soc.*, 2012, **134**, 15016–15021.

21 W. Lu, D. Yuan, J. Sculley, D. Zhao, R. Krishna and H.-C. Zhou, *J. Am. Chem. Soc.*, 2011, **133**, 18126–18129.
22 W. Lu, J. P. Sculley, D. Yuan, R. Krishna, Z. Wei and H. C. Zhou, *Angew. Chem., Int. Ed.*, 2012, **51**, 7480–7484.
23 M. H. Weston, O. K. Farha, B. G. Hauser, J. T. Hupp and S. T. Nguyen, *Chem. Mater.*, 2012, **24**, 1292–1296.
24 K. Sumida, D. L. Rogow, J. A. Mason, T. M. McDonald, E. D. Bloch, Z. R. Herm, T.-H. Bae and J. R. Long, *Chem. Rev.*, 2012, **112**, 724–781.